The Nucleation, Alloying, and Stability of Co-Re Bimetallic Nanoparticles on Al_2O_3/NiAl(110)

*Rik Mom,[1‡†] Oleksii Ivashenko,[2‡] Joost W.M. Frenken,[1,††] Irene M.N. Groot,[1,3] Anja O. Sjåstad[2]**

[1] Huygens-Kamerlingh-Onnes Laboratory, P.O. Box 9504, 2300 RA Leiden, the Netherlands

[2] Chemistry department and Centre for Materials Science and Nanotechnology of University of Oslo, Sem Sælands vei 26, 0371 Oslo, Norway

[3] Leiden Institute of Chemistry, P.O. Box 9502, 2300 RA Leiden, the Netherlands

† Present address: Department of Inorganic Chemistry, Fritz-Haber-Institut der Max-Planck-Gesellschaft, Faradayweg 4-6, 14195 Berlin, Germany

†† Present address: Advanced Research Center for Nanolithography, Science Park 110, 1098 XG Amsterdam, The Netherlands

‡ These authors contributed to the manuscript equally

ABSTRACT

This paper reports on preparation and characterization of nanostructured Re and Co-Re/Al_2O_3/NiAl(110) surfaces designed as model catalysts for operando studies of Fischer-Tropsch synthesis. Scanning tunneling microscopy on pure Re particles identified strong Re-Al_2O_3 support

interaction, resulting in uniform nucleation and growth on random point defects. X-ray photoelectron spectroscopy confirmed the strong interaction through a shift in the binding energy, in addition to size-dependent final state effects. Co-Re particles were prepared by sequential deposition of the two metals, resulting in core-shell structures in which the shell was (strongly) enriched with the metal deposited second. Annealing of bimetallic particles allowed for elemental redistribution, as was concluded from the XPS data and supported by modeling. The annealing also resulted in sintering of bimetallic clusters. Interestingly, the thermal stability of the Co-Re surfaces prepared by sequential deposition of Co, followed by Re, was better than that of both pure Co and pure Re.

Introduction

Fischer-Tropsch (FT) synthesis is a powerful process to catalytically convert synthesis gas (syngas: H_2 + CO) to synthetic fuels. Commercially used catalysts often consist of supported Fe or Co nanoparticles (NPs); the latter being particularly suited for syngas conversion obtained from natural gas reforming.[1] Cobalt-based catalysts give paraffins and some α-olefins as the main products.[1] Industrial FT catalysts frequently contain small quantities of metals as Re, Pt, or Ru, which boost catalyst activity, product selectivity, and lifetime. Furthermore, promoters dictate the dispersion, reducibility, and particle size of the most important constituent of the catalyst: e.g. as discussed for the metallic Co nanoparticle component.[2-4] The current success of the FT technology is a result of painstaking trial-and error work, i.e. correlating catalyst parameters such as preparation method, particle size distribution, and/or oxidation state with performance data. Unfortunately, fundamental and operando approaches to unravel the underlying mechanism of the Co-promoted FT catalyst are less developed. In this perspective, detailed investigations on powders (3D) and surfaces (2D) using tools that give detailed information on both bulk properties

as well as the top few atomic layers of the catalyst at operative conditions are vital. In this regard, a fundamental study was recently performed in our laboratories by Navarro et al., showing accumulation of hydrocarbon chains of 14 or 15 carbon atoms on the Co(0001) surface using operando STM at 220 ^{o}C in a 2 H_2 + CO gas mixture at 2 bar.[5]

Although the superior performance of Re-promoted Co catalysts in FT synthesis is well established,[3-4] the location of the Re atoms in the Co nanoparticles is still debated. Some studies state that Co and Re form an alloy, others propose that single Re atoms accumulate on the surface in intimate contact with Co metal atoms or that Re is located just below the Co nanoparticle surface.[6-8] In this connection, we recently reported that Re can mix with Co on the nanoscale when using a colloidal synthesis approach, and that as much as 15 at. % Re can be incorporated into Co NPs, taking the β-Mn-type structure, as a solid solution (alloy).[9]

To unravel fine structural and mechanistic details taking place on the real Co-Re-supported 3D catalyst surface during FT synthesis, precise, well-defined 2D model catalysts are essential. Al_2O_3 is a common support for Co-based FT catalysts, and a 2D alumina support can be easily grown on a NiAl(110) single crystal by mild oxidation forming a sub-nm thick film,[10-11] providing sufficient electric conductivity for ultrahigh vacuum (UHV) techniques such as X-ray photoelectron spectroscopy (XPS) and scanning tunneling microscopy (STM) and their operando versions, near-ambient pressure XPS and high-pressure STM.

The preparation and characterization of nanoparticles grown on Al_2O_3/NiAl(110) is widely reported in the literature, including un-promoted Co/Al_2O_3/NiAl(110).[12-14] In brief, defects of the alumina film play a dominant role on the nucleation behavior of metal NPs. Furthermore, metal-support interaction determines which of the nucleation sites (point defects, domain boundaries, or step edges) will exhibit preferential growth.[13] In contrast to the case of reducible oxide support,

the oxidation state of the deposited metal particles is less likely to be affected by interaction with the support.[15] In particular, Co nucleates preferentially on step edges and domain boundaries in 3D fashion forming rounded nanoparticles (contact angle >90°).[14] Annealing to temperatures of 500-900 K leads to particle sintering and migration of Co into the subsurface region.[16]

To the best of our knowledge no similar investigations have been undertaken for the case of Re or bimetallic Co-Re on Al_2O_3/NiAl(110). In this paper we are utilizing STM and XPS as the main characterization tools to report for the first time on the nucleation and growth of Re and bimetallic Co-Re NPs deposited on Al_2O_3/NiAl(110). We investigate the metal-support interaction, the chemical state of Co and Re in the as-prepared bimetallic NPs, and the Co-Re element distribution, including the effect of temperature on sintering and elemental restructuring. We foresee the obtained results to be particularly useful in the preparation of well-defined 2D model catalysts suited for exploring the fine details of Co-Re/Al_2O_3 catalysts for Fischer-Tropsch synthesis.

Experimental part

All experiments were carried out in a home-built UHV setup described elsewhere.[17] The system is equipped with an X-ray photoelectron spectrometer (SPECS Phoibos), an electron-beam evaporator (Oxford Applied Research), standard sample preparation equipment, and a custom-made scanning tunneling microscope.

Sample Preparation

The NiAl(110) single crystal (Surface Preparation Laboratory[18]) was cleaned by cycles of 1.5 kV Ar^+ sputtering and annealing at 1300 K. Growth of the alumina film was accomplished according to a literature procedure.[10] In brief, the growth was performed by three cycles of oxidation at 600 K in a 5×10^{-6} mbar O_2 background (1×10^{-6} mbar O_2 in the last cycle) for 10 min and subsequent UHV annealing at 1100 K (1050 K in the last cycle) for 5 min.[11] The cleanness,

flatness and absence of adsorbates on the film were checked by XPS and STM, respectively. The cobalt, rhenium and mixed nanoparticles on alumina were prepared using an electron-beam evaporator. All depositions were carried out with the Al_2O_3/NiAl(110) support at room temperature. Re (99.97 %, ChemPUR) and Co (99.99 %, ChemPUR) evaporation was conducted in UHV at pressures better than 2×10^{-9} mbar, using fluxes of 0.004 monolayer (ML)/min and 0.3 ML/min, respectively, as estimated from STM images (see particle statistics paragraph below for the procedure). Annealing of surfaces was carried out at pressures better than 2×10^{-9} mbar. Each temperature was maintained for 30 min. The sample temperature was calibrated according to the procedure described previously, using a thermocouple welded to the side of the sample.[19]

X-ray Photoelectron Spectroscopy

All XPS experiments were carried out using a monochromated Al Kα X-ray source with a 54° incidence angle from the surface normal and electron collection along the surface normal. The analyzer pass energy was 10 eV, dwell time 0.1 s. The spectra were analyzed using the least-squares curve fitting program Winspec.[20] Binding energies are determined by peak fitting procedure and are reported with an uncertainty of ± 0.1 eV, referenced to the Ni $2p_{3/2}$ and Al metal $2p_{3/2}$ photoemission peaks centered at 852.7 eV and 72.9 eV, originating from the substrate. Fitting of the Re 4*f* and of the (Ni3*p*Al2*p*) spectra included a Shirley baseline subtraction and fitting with a convolution of Gaussian and Lorentzian functions. A Ni 2*p* reference spectrum, measured on a clean, unmodified Al_2O_3/NiAl(110) surface before Co deposition, was subtracted from all Co 2*p* spectra. Experimental Re and Co signal attenuation is normalized to the Ni3*p*Al2*p* intensity and has an estimated uncertainty of 2%, based on analysis of uncertainties described in SI section 7.

STM measurements

Scanning tunneling microscopy was conducted using cut $Pt_{80}Ir_{20}$ 0.25 mm diameter tips (Goodfellow). The data were recorded using the CAMERA 4.3 software package developed at Leiden University.[21,22] Imaging was performed at a typical sample bias of −1 V and tunneling current of 0.2 nA. Particle heights are reported with an uncertainty of ± 0.03 nm, according to calculations in SI section 7.

Particle Statistics

Statistics on cluster density, coverage, and height of the particles were obtained using the Gwyddion software package.[23] Errors found in the automated particle recognition were corrected in manual post-processing. For statistical analysis, only image segments without steps on the surface were considered. Particle heights were determined from particle height histograms, which were fitted with a Gaussian function. The typical distribution width obtained from the Gaussian fit was 0.25 nm.

A combination of STM and XPS results was used to determine the Re and Co coverage. The Re 4*f*/(Al 2*p* + Ni 3*p*) and Co 2*p*/(Al 2*p* + Ni 3*p*) ratios were determined for all experiments. To obtain the metal coverage from an STM image, the total volume of the particles in the image was calculated using particle detection via thresholding. Due to 0.3 nm overestimation of heights of metallic particles on Al_2O_3/NiAl(110) at the sample bias used in this work (−1 V),[14] the volume was calculated with respect to the horizontal plane defined by the 0.3 nm threshold. Due to overestimation of the lateral dimensions of the particles a volume overestimation between 2.1× and 17.0× can be observed (see Supporting Information in Ref. 11). Assuming the tip radius to be of similar size as the particles, we have divided the total volume obtained by the thresholding method by four,[11] obtaining coverage values consistent with literature on Co/Al_2O_3/NiAl (110). After calibration of the XPS (Re 4*f* or Co 2*p*) /(Al 2*p* + Ni 3*p*) ratio versus STM coverage, a

coverage estimate could also be obtained from XPS intensities for the bimetallic samples. Similarly, particle volumes were calculated using the XPS coverage and the particle density obtained from STM. While the particle volumes could also be determined directly from the STM data, the combined XPS/STM procedure minimizes the influence of the variations in tip size. All coverages are expressed in monolayers of the Re(0001) and Co(0001) surfaces; 1 Re ML corresponds to 1.52×10^{15} Re atoms/cm^2 and 1 Co ML is equal to 1.83×10^{15} Co atoms/cm^2. All particle heights reported here are the actual particle heights, determined as (observed particle height minus 0.3 nm). Throughout analysis particle height (h) was used as the most reliable indication of particle size, since STM is more sensitive in the normal direction. Contact angles and work of adhesion were estimated following an approach described elsewhere.[14] Error bars for cluster height and cluster density were estimated as detailed in the Supporting Information.

Results and discussion

Co and Re nucleation on alumina

The alumina support used in this work is a two-layer alumina film, see **Figure 1**a.[10,24] Despite the fact that the grown film is highly crystalline, it does contain point defects and domains with different orientations (see the dark lines in Figure 1a). Because the bonding in the alumina film is highly saturated,[24] nucleation of metallic nanoparticles deposited on Al_2O_3/NiAl(110) predominantly occurs on point defects, domain boundaries, and step edges.[11-14, 25-26] The relative importance of these three nucleation sites is determined by the metal-support interaction strength.[11, 13, 27] If the interaction strength is high, metal atoms arriving on the surface are likely to form a nucleus on one of the first defects they encounter. Since the point defects are randomly distributed, in contrast to the domain boundaries and step edges, the first defects encountered by the arriving metal atoms are often the point defects. Hence, metals with a strong metal-support

interaction tend to nucleate predominantly on point defects. In contrast, weakly adsorbed metal atoms will travel further before nucleating, and will therefore show a preference for the nucleation site that binds stronger. In the case of our alumina film, the strong binding sites are the domain boundaries and step edges.

Figure 1b shows the sample after deposition of 0.3 ML Co at room temperature. In good agreement with literature results,[13-14] we find that point defect nucleation at random terrace sites is common, yet there is a preference for the step edges (**Figure S1**). This is consistent with an intermediate metal-support interaction, in which the atoms arriving on the surface only sometimes stick to the point defects for long enough to form a nucleus with another Co atom, but often not, allowing the atoms to proceed to the stronger binding step edges and domain boundaries. Corroborating this assignment, the particle density is 9×10^{12} cm^{-2}, which is close to the saturation density of noble metals on this support,[13, 28] but lower than that observed for vanadium.[26] We should point out that the deposition flux is an important parameter in the nucleation process, as a high deposition flux tends to result in a high particle density.[27] In a typical experiment, Co was deposited at a high flux of 0.3 ML/min, and therefore the resulting particle densities obtained were slightly larger than those reported in earlier work.[14]

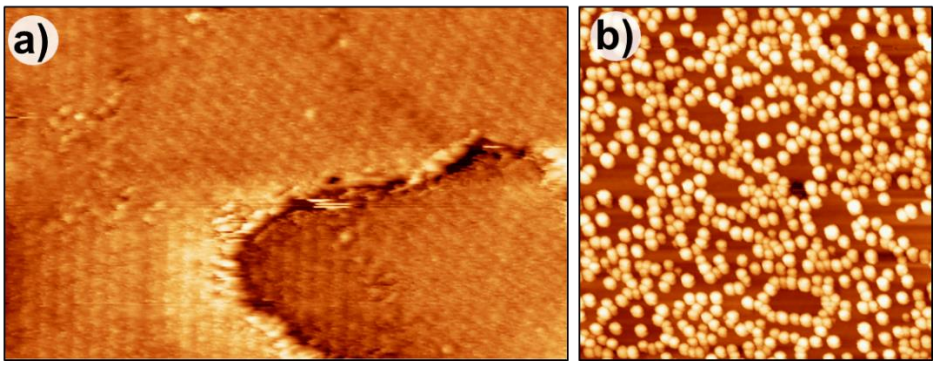

Figure 1. a) STM topography image of a 0.5 nm thick alumina film grown on a NiAl(110) single crystal, showing a step edge and domain boundaries (dark lines). Image size 32×20 nm^2, U_s –0.7

V, I_t 0.1 nA. b) STM topography image of 0.3 ML Co/Al_2O_3/NiAl(110) showing random nucleation on alumina terraces and domain boundaries, and decoration of step edges. Image size 80×80 nm^2, U_s –1 V, I_t 0.2 nA.

Based on the average particle height (h = 0.84 nm) and average particle volume (V = 0.65 nm^3) we can get a rough estimate of the contact angle α of the particles by approximating them as (truncated) spheres:[14]

$$\cos\alpha = 1 - \frac{3\pi h^3}{3V + \pi h^3}, \qquad (1)$$

For the very small particles used in this work, the assumption of (truncated) spheroid particles is a crude one. Hence, the value of α should be seen as indicator for the tendency to form flat or rounded particles rather than as an accurate descriptor of the particle shape. Similarly, the macroscopic formula for the work of adhesion yields a rough indication of the particle-support interaction:[14]

$$W_{ad} = \gamma(1 + cos\ \alpha) \qquad (2)$$

In equation 2, γ is the surface free energy of the metal. Taking into account the larger surface area of the particles with respect to our spheroid approximation (estimated 10% larger), we used γ = 2.78 J/m^2.[29] Inserting the values for h and V in Equation 1 and 2, we find a contact angle of 118° and a work of adhesion of 1.5 J/m^2, in good agreement with the literature[9] value of 1.6-1.8 J/m^2.

Rhenium is a much more oxophilic metal than Co, and hence one would expect a strong Re-support interaction.[30] **Figure 2** shows that this is indeed the case. The particle density at 0.4 ML is 12.8×10^{12} cm^{-2} (Table 1), which is comparable to the highest density for metals deposited at room temperature on Al_2O_3/NiAl(110).[13] The particles are nearly completely randomly dispersed, implying that nucleation preferably takes place at point defects rather than at the step edges. The

strong Re-support interaction is also apparent from the contact angle of 103° (for 0.4 ML Re) and work of adhesion 3.1 J/m^2, which is twice that for Co for comparable coverage.

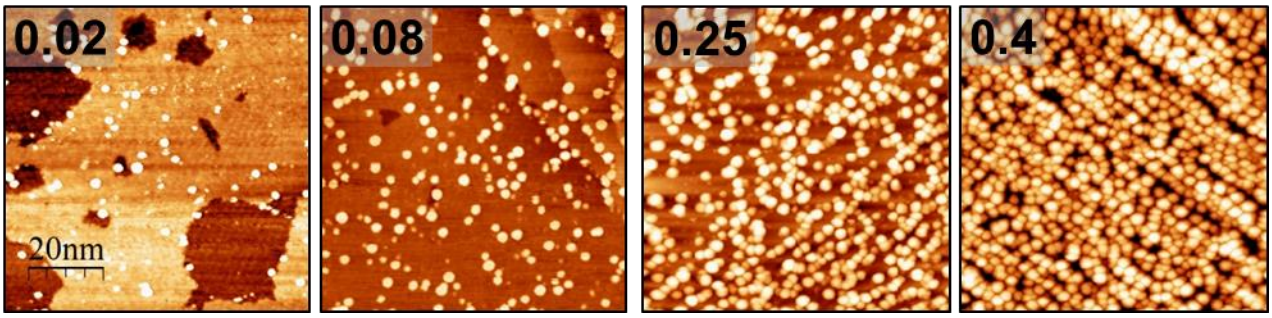

Figure 2. Series of STM images for increasing Re coverage (0.02-0.4 ML) on Al_2O_3/NiAl(110), showing almost no preference for nucleation on steps or domain boundaries. All images are 80×80 nm^2, U_s −1 V, I_t 0.2 nA.

Table 1. Particle density, volume, height and position of the Re 4$f_{7/2}$ XPS peak for a series of Re coverages on Al_2O_3/NiAl(110).

Coverage (ML)	Density (10^{12}clusters cm^{-2})	Average particle volume (nm^3)	Height (nm)	Re 4$f_{7/2}$ (eV)
0.02	1.2	0.3	0.4	42.4
0.04	2.2	0.3	0.5	42.1
0.08	2.5	0.3	0.5	42.0
0.10	4.4	0.7	0.7	41.8
0.25	8.6	1.4	0.8	41.6
0.40	12.8	1.2	0.8	41.4
Bulk metal				40.5 [31-32]

To obtain information on the electronic state of the Re particles, we conducted XPS measurements. **Figure 3** and **Table 1** show that the Re 4*f* binding energy is strongly dependent on the particle height (h) and volume (Figure S4). For the lowest coverage of 0.02 ML, the 4$f_{7/2}$ peak was found at 42.4 eV, shifted to higher binding energy by ca. 2 eV from its literature bulk value of 40.5±0.2 eV.[31-32] Although binding energy shifts with respect to the bulk metal are commonly

observed for nanoparticles,[33-36] especially for subnanometer ones, the magnitude of the shift is relatively large. As the coverage was stepwise increased to 0.4 ML, the $4f_{7/2}$ peak position progressively moved to 41.4 eV, with a concomitant peak FWHM narrowing from 3.5 to 1.8 eV. Figure 3b compares our results for the Re4*f* binding energy shift as a function of particle size to those obtained by Richter *et al.* on $Co/Al_2O_3/NiAl(110)$.[34] Like Richter *et al.*, we obtained the particle size by assuming the particles to be hemispheres, in reasonable agreement with the observed wetting angle. For the same size, the binding energy shift of the Re particles is some 0.3 eV higher than that of Co (Figure 3b).

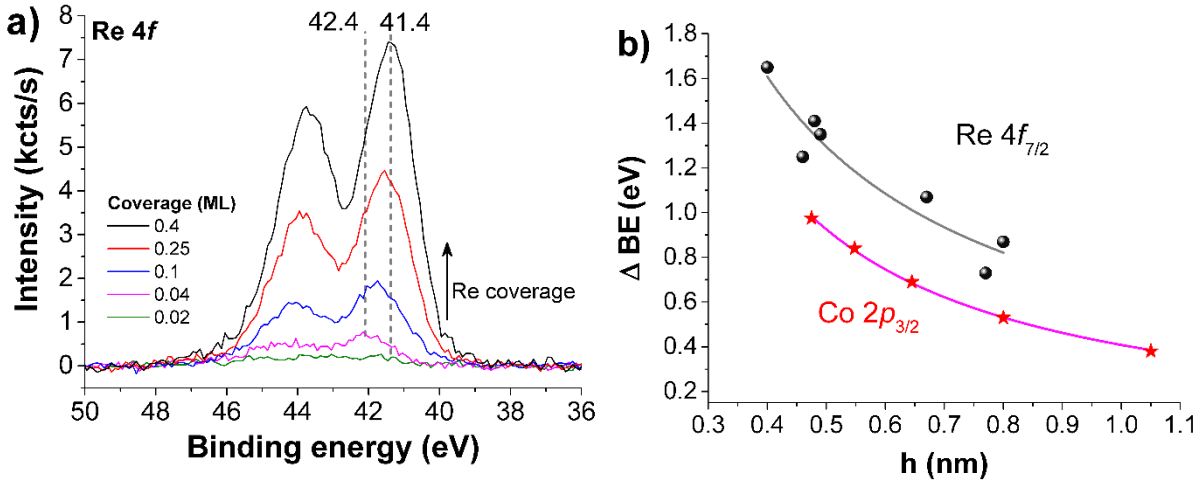

Figure 3. a) Rhenium 4*f* core level photoelectron spectra for increasing Re coverage of 0.02-0.4 ML. b) Binding energy shift as a function of particle height for Re ($4f_{7/2}$) (black spheres) and Co ($2p_{3/2}$) (stars). Co data were extracted from Richter *et al.*[34] A 1/r fit is also shown for both data sets. See also Figure S4 for normalized Re 4*f* spectra and ΔBE plotted on "particle volume" axis.

Three main causes for the size-dependent binding energy shifts can be identified: a) Finite size effects. Due to the limited size of the particles, the average coordination number decreased, causing lattice strain. Furthermore, the density of states in the particle is decreased due to the limited number of electrons it contains. These effects alter the electronic properties of the metal, and hence

the (initial state) core level binding energy.[33-36] b) Support effects. The interaction with the support can lead to charge transfer from the particle to the support, resulting in shifts (e.g. –0.7 eV for platinum on ceria) towards the bulk position as the particle size increases from 0 to 2.5 nm.[37] Additionally, the support may donate oxygen atoms to the particles, increasing their oxidation state. As aluminum is substantially more oxophilic than rhenium,[30] we do not expect such an oxidation-reduction reaction to occur. c) Final state effects. These occur due to incomplete screening of the core hole created during photo-ionization when particles are supported on non-conductive substrates.[33-34] To fill the core hole in a nanoparticle the electrons therefore need to tunnel from the NiAl(110) substrate through the bandgap of alumina to the particle, which is slow with respect to the photo-ionization process.[12]

Using an Auger parameter analysis, Richter *et al.* separated the final state effect from the initial state contributions due to finite particle sizes and support interactions. While the final state effect was found to dominate, a contribution of around 0.3 eV from the initial state effect was observed, with a minor dependence on particle size within the investigated range. Because the Co and Re particles are both metallic, for comparable sizes of particles we expect the final state effect to be almost identical.[33] Hence, the difference between the results for Re and Co likely stems from initial state contributions. Richter *et al.* identified the effect of finite particle size as the major cause for the 0.3 eV shift observed for Co (at maximum studied coverage), noting that the alumina film is a weakly interacting support. In the case of Re, stronger interaction with the support most likely justifies the additional 0.3 eV shift observed in XPS.

Sequential deposition of Re and Co

Co-Re particles were prepared by two sequential deposition procedures. In the first, 0.1 ML Re was deposited, followed by 0.4 ML Co (see **Figure 4**a, referred to as Re+Co hereafter). In the

second procedure, 0.3 ML Co was deposited first, followed by 0.4 ML Re (see Figure 4b, referred to as Co+Re hereafter). The peak position of the Re 4*f* doublet for both the Re+Co and Co+Re particles was found at 41.3 eV, shifted equally from its "bulk" metal reference, in contrast to pure 0.1 ML Re on alumina observed at 42.0 eV. The equal shift implies that the Re is associated with Co in both cases, regardless of evaporation order. A more detailed description comes from the measured particle densities after the first and second stage of deposition. For the Re+Co sample, there is an increase in the particle density from 2.9×10^{12} to 12.3×10^{12} cm^{-2} between the Re and Co deposition. This indicates that the Co is not only associated with the Re, but that pure Co particles have been formed as well. In contrast, when the deposition order was reversed for the case of Co+Re, the particle density remained more or less constant (9.0×10^{12} and 8.2×10^{12} cm^{-2} respectively), indicating that all particles are bimetallic Co-Re. In contrast, for smaller Re coverage, i.e. 0.3 ML Co + 0.05 ML Re, pure Co and bimetallic Co+Re particles were formed (Figure S2).

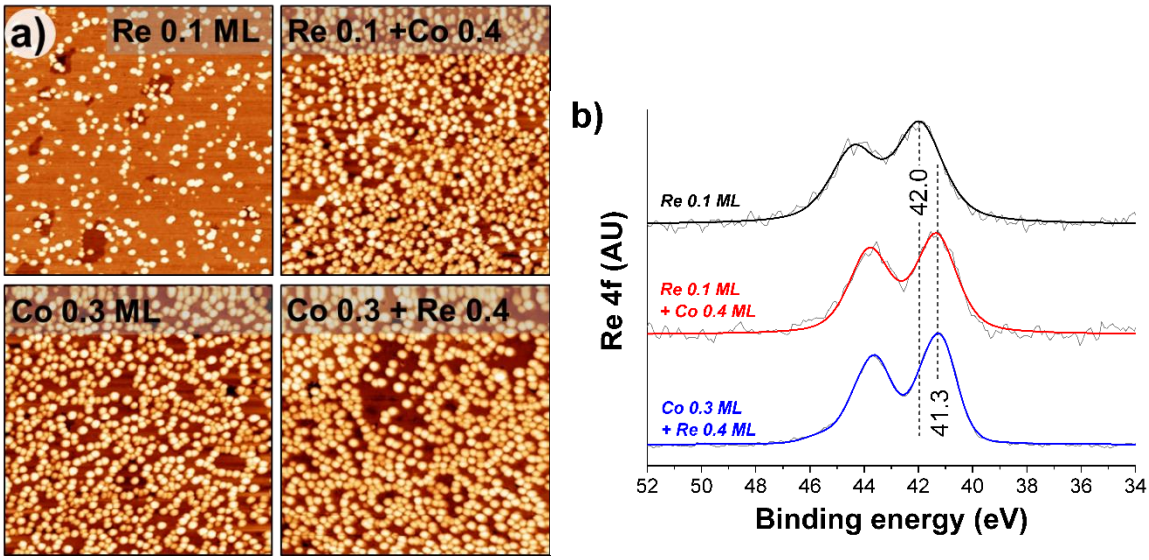

Figure 4. a) 100×100 nm^2 STM topography images corresponding to sequential deposition of 0.1 ML of Re followed by 0.4 ML of Co (a, top); and sequential deposition of 0.3 ML of Co followed

by 0.4 ML of Re (a, bottom). U_s −1 V, I_t 0.2 nA. b) Corresponding Re 4*f* spectra for 0.1 ML Re/Al_2O_3/NiAl(110) before and after deposition of 0.4 ML of Co, showing a shift of the Re doublet due to association with Co (top black and middle red lines). A similar normalized spectrum was obtained when 0.4 ML Re was evaporated on top of 0.3 ML of Co (bottom blue line).

To investigate the distribution of Co and Re in the particles, we analyzed the Re 4*f* and Co $2p_{3/2}$ peak intensities after the first and second stage of the preparation, **Figure 5** (see also Table S1). In both the Re+Co and the Co+Re case, the XPS signal of the metal that was deposited first is attenuated due to the second deposition. This attenuation results from the increase in size of the particles, which increases the average length that the photoelectrons have to travel through the particle before escaping into vacuum. We modeled such attenuation for two scenarios: 1) A particle with an overlayer of the second metal on the first metal (core-shell model). 2) The first and second metal forming a particle with mixing of the two elements (alloy model). The details of the models can be found in the Supporting Information. We point out that other Co/Re distribution models may be possible.[6-7] Hence, the comparison of the models chosen here to the experimental data should only be used to estimate the tendency of Co/Re interdiffusion within a particle. **Figure 5** compares predicted attenuation of XPS intensities for core-shell and alloyed nanoparticles scenarios for bimetallic Re+Co (left) and Co+Re (right) nanoparticles with a 0-0.5 nm overlayer of the second metal with experimental data for 0.24 nm Co overlayer and 0.12 nm and 0.32 nm Re overlayer, respectively. These overlayer thicknesses were determined using the change in particle height following the deposition of the second metal (see Table S1 in the Supporting Information).

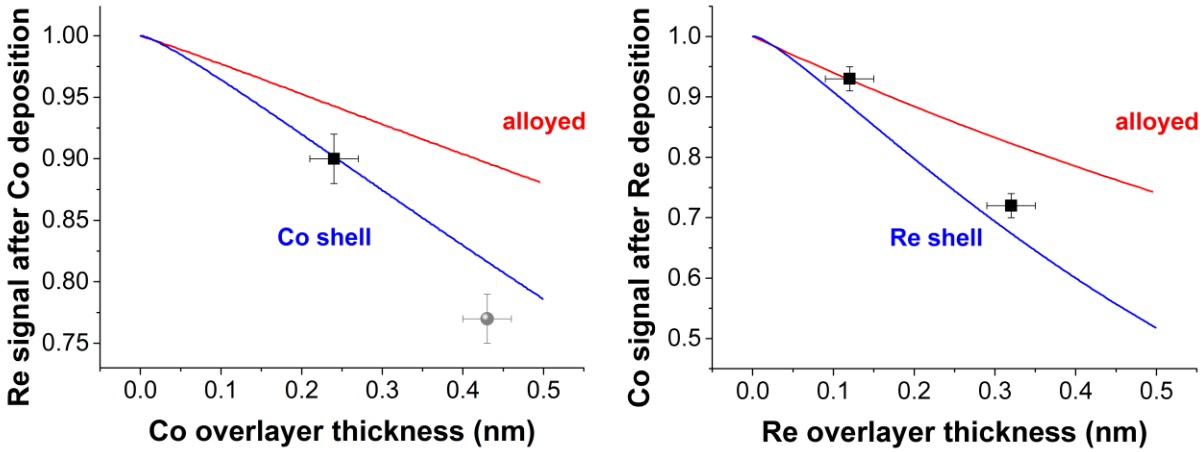

Figure 5. Comparison of XPS attenuation modeling and experimental data points for 0.05 ML Re + 0.2 ML Co at room temperature and after annealing at 750 K (left) and 0.3 ML Co + 0.05 ML Re, + 0.35 ML Re at room temperature (right). The modeled attenuation of the initially evaporated metal in a core-shell configuration is plotted in blue, and for an alloyed particle in red. Experimental data points obtained as prepared at RT are plotted as black squares, and the Re attenuation after annealing to 750 K in a) is plotted as a grey sphere (further details are in the Effects of annealing section). Error bars for experimental datapoints represent the errors in determining particle height and XPS peak area ratios and were calculated as described in the SI. The experimental overlayer thicknesses were calculated using the particle height data provided in Table S1 in the SI.

In general, alloyed nanoparticles imply mixing of the metals and therefore exhibit less attenuation of the first metal, while in the core-shell structure the core is more attenuated due to an overlayer. For the case of Re+Co, **Figure 5**, left panel indicates that the experimental Re 4*f* attenuation (0.90) is well described by the core-shell model, whereas the alloy model is somewhat off (0.94). Taking into account an error margin of 2% in the XPS intensity, and 0.03 nm in the STM height estimation, the offset of the alloy model is just outside the estimated uncertainty range.

Thus, we establish that the Re+Co sample tends to form Re core, Co shell particles. In contrast, we are inclined to state that the deposition of 0.05 ML Re on Co results in alloy formation, although the difference between the two models is almost within the uncertainty of the modeled Co attenuation (right panel). For further addition of Re up to 0.4 ML, the model neither predict core-shell nor alloy formation. To be more conclusive, we find that the wetting angle of the 0.3 ML Co + 0.4 ML Re particles is 132°, which is larger than 118° observed for pure Co. Assuming that the particle-support interaction W_{ad} has remained constant, this indicates an increase in the particle's surface free energy γ (see Equation 2). For Co core - Re shell particles, this is to be expected, because the Re surface free energy (3.97 J/m^2) is significantly larger than that of Co (2.78 J/m^2).[29] Therefore, we suggest that the 0.3 ML Co + 0.4 ML Re particles form a core-shell structure.

Since the order of the Co and Re deposition affects the distribution of Co and Re within the particles, we can conclude that the internal equilibration of Co-Re particles is hampered at room temperature. This kinetic limitation, within days of sample preparation, is often observed in room temperature nano-alloying studies.[14, 38-39] If the metal with the lowest surface free energy is deposited second, it forms an overlayer, even if the metals tend to form homogeneous alloys in bulk (such as the Co-Re system[40,41]). In contrast, when the metal with the highest surface energy is deposited second, partial or complete segregation of the first deposited metal occurs.

Effects of annealing

To study the thermal stability of the model catalysts and get more insight into the restructuring of the bimetallic particles at higher temperature, we conducted a series of stepwise annealing experiments. At each step, the temperature was maintained for 30 minutes, after which we performed STM imaging (**Figure 6** and **Figure S3** in the Supporting Information) and XPS quantification (**Figure 7**c) at room temperature.

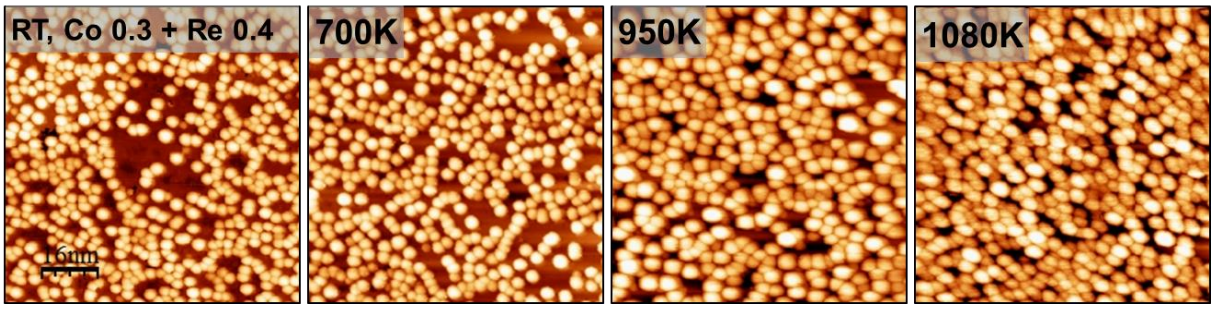

Figure 6. Series of STM images for bimetallic nanoparticles (Co+Re, 0.3+0.4 ML) measured at room temperature as prepared at room temperature, annealed at 700 K, 950 K, 1080 K. Scale 80×80 nm^2, U_s –1 V, I_t 0.2 nA.

From STM images shown in **Figure 6** and **S3,** the normalized particle densities and heights for pure Re, Co+Re, and Re+Co versus annealing temperature were extracted and presented in **Figure 7a,b** (see SI for plots without normalization), which are compared to earlier work by Heemeier *et al.* on pure Co/Al_2O_3/NiAl(110).[16] From the decrease in cluster density and the increase in cluster height upon annealing it becomes clear that sintering occurs in all cases, but there are differences in the degree of sintering. For Pd, Rh, and Co on Al_2O_3/NiAl(110), Heemeier *et al.* found only small differences in the extent of sintering.[16] In line with this, we find that pure Re shows a similar degree of sintering as pure Co. The Re+Co sample, which predominantly consists of pure Co particles, also follows the trend of pure Co. It should be noted that the particle size and density may affect the sintering rate. However, based on the similarity between the high density Re+Co sample (12.3×10^{12} cm^{-2} initially) and the low density Co sample (3.3×10^{12} cm^{-2} initially) of Heemeier *et al.*,[16] these effects appear to be of lesser importance.

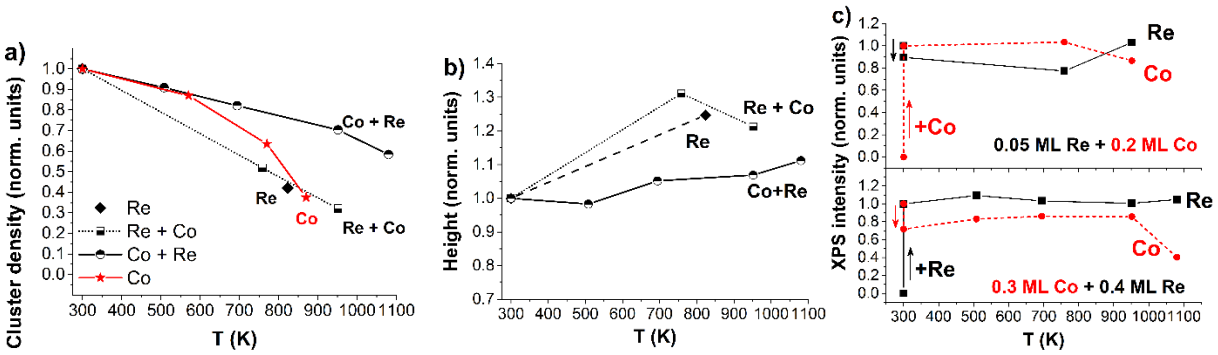

Figure 7. Normalized cluster density a) and cluster height b) as a function of annealing temperature for pure Re (diamonds), Re+Co (squares) and Co+Re (circles) on Al_2O_3/NiAl(110). The dataset for pure Co/Al_2O_3/NiAl(110) from Heemeier *et al.* is plotted for comparison (red stars).[16] The normalization was performed with respect to the situation at room temperature. c) Normalized XPS intensity of Re4*f*/(Ni 3*p* + Al 2*p*) and Co2*p*/(Ni 3*p* + Al 2*p*) core levels for 0.05 ML Re + 0.2 ML Co (top panel) and 0.3 ML Co + 0.4 ML Re (bottom panel) as a function of annealing temperature. For normalization, the intensity after deposition of the first metal is taken as 1.

The Co-Re particles produced by the Co+Re deposition are much more stable than pure Co or Re. To explain this, we note that three particle/material properties can affect sintering: 1) The detachment barrier to release atoms from the particles (Ostwald ripening mechanism); 2) The diffusion barrier of particles as a whole (coalescence mechanism); 3) The diffusion barrier of detached atoms (Ostwald ripening). Since the atoms detaching from Co-Re particles are the same as for pure Re or Co, the sintering resistance of Co-Re cannot be explained by the Co or Re atomic diffusion barrier (3). Hence, either the detachment barrier (1) or the particle diffusion barrier (2) is higher for the bimetallic particles than for the pure metals. If the Co-Re particles were able to diffuse as a whole, one would expect that in addition to sintering, also relocation of particles towards oxide domain boundaries and step edges would occur, since these bind the particles more strongly. However, the images in Figure 6 do not show an increased preference for step edges or

domain boundaries. Therefore, we conclude that the stability of the Co-Re particles results from a high detachment barrier (1). This conclusion implies that there is a favorable interaction between Co and Re, which is supported by the study of solid solutions over the entire composition range in the Co-Re binary alloy phase diagram.[40]

Besides sintering, the annealing affects the elemental composition of the particles, and the Co-Re distribution within the particles. Already at temperatures as low as 508 K, changes in the relative Co $2p_{3/2}$ and Re 4*f* intensities are observed (see Figure 7c). This confirms our conclusion from the previous section that Co-Re interdiffusion is kinetically hindered during the preparation at room temperature (see above).

For the Re 0.05 ML + Co 0.2 ML experiment, the as-prepared sample is a mix of pure Co particles and Re core-Co shell particles. During sintering at 750 K, the Re signal drops from 90% to 77% (with respect to bare 0.05 ML Re), as shown in the top panel of Figure 7c. This suggests that Re remains in the particle core, while the Co shell thickens (height increase of 0.43 nm). In good agreement with the core-shell description, we find a Re signal of 82% with respect to bare Re using the core-shell model (h=0.43 nm in Figure 5, left). Hence, little or no Re-Co intermixing occurs at 750 K. Similar to our observations, Parschau *et al.* showed that alloying of Co deposited on Re(0001) only occurs in the interface layer within the investigated temperature range up to 500 K.[42] At 950 K, the Re signal is completely recovered, while the Co signal decays. At such high temperatures, diffusion of metal atoms into the substrate becomes possible at the domain boundaries.[16] The height decrease of the particles and the loss of Co in the XPS signal in Figure 7c confirm that some of the Co is indeed removed from the surface. We should point out that evaporation of Co does not play a role at the temperatures employed here.[43] Since the Re signal for Re+Co completely recovers to its intensity before Co deposition, the Re atoms do not diffuse

into the substrate at 950 K. Similar behavior is observed for the Co+Re sample (Figure 7c, bottom panel), although at higher temperature (1080 K). The difference in onset temperature was attributed to the higher Re content in the Co+Re sample, which likely increases the stabilizing Co-Re interaction. Note that for the Re+Co sample, most of the Co remained on top of the substrate. Hence, the complete recovery of the Re signal indicates that Re has moved from the core of the particles towards the surface.

For Co+Re, the Co signal regains intensity during annealing up to 950 K (see Figure 7c, bottom part). This could be interpreted as the result of Co penetrating the Re shell, moving closer to the particle surface. Remarkably however, the Re intensity remains steady for Co+Re over the entire temperature range probed here. This suggests that the retrieval of the Co signal is not due to alloying of the Co core with the Re shell, as the Re signal would be attenuated in this case. Indeed, our model indicates a Re attenuation of 19% in case of homogeneous alloy formation (based on the data at 508 K, see supporting information for details on the model) with respect to a pure core-shell situation. Therefore, the simple model applied for the room temperature situation is not suited to explain the element distribution in the post-annealed Co-Re NPs.

Nevertheless, some hints regarding the more detailed arrangement of Co and Re in the annealed particles can be obtained from the literature and additional modeling of our XPS data. Based on low energy ion scattering data and density functional theory calculations, Bakken *et al.* proposed that Re occupies subsurface positions inside the Co-Re particles, instead of forming a homogeneous alloy.[8] Stimulated by this idea, we modeled subsurface Re in the particles using a Co-Re-Co sandwich structure (see supporting information for more details). This results in a small Re attenuation of 8% (based on the data at 508 K), which comes significantly closer to the experimentally observed stable Re signal, particularly considering that the Co+Re sample prepared

at room temperature already showed some Co-Re mixing. Meanwhile, the Co attenuation decreases to 21%, which is also fairly consistent with the experimental data (17%). Hence, the Re subsurface structure appears to be a reasonable explanation of our data. However, further study is required to exclude the possibility of other complex Co-Re arrangements.

Conclusions

Motivated to prepare a well-defined Co-Re/Al_2O_3 model catalyst for Fischer-Tropsch synthesis, we provide the first report on the nucleation and growth of Re and Co-Re clusters on Al_2O_3/NiAl(110), including a detailed study of the effect of annealing on the particle distribution and element distribution within the particles. In contrast to Co, which has medium metal-support interaction and tends to nucleate at domain boundaries and step edges, we find that Re exhibits strong metal-support interaction (twice higher work of adhesion). This results in high particle densities and growth of Re clusters at randomly distributed point defects. A cluster size effect on the binding energy was observed for both Co and Re using XPS. Due to the stronger metal-support interaction of Re, its binding energy shift was higher by +0.3 eV compared to Co.

Sequential deposition of Co and Re at room temperature yields un-equilibrated core-shell Co-Re and Re-Co bimetallic particles, depending on evaporation order. When Co is promoted with small quantities of Re (Co+Re) an alloy formation can be observed, as predicted earlier.[44] Post-annealing enables internal elemental redistribution to occur. The equilibrated structure cannot be satisfactory modeled as a homogeneous alloy or a core-shell structure, yet could be explained by the Co core - Re subsurface layer - Co shell structure suggested in the literature. [8, 45]

The elemental redistribution of the clusters due to annealing is accompanied by sintering for bimetallic particles. For Re, the sintering results are similar to the case of pure Co reported in the literature.[16] For the bimetallic Co-Re particles (produced via deposition of Co followed by Re

deposition), superior sintering resistance is observed. We attribute this to a higher adatom detachment barrier for the bimetallic nanoparticles, due to the increased stability of both Co and Re in the bimetallic particles with respect to their pure phases.

The currently developed nanostructures are targeted to mimic real industrial Fischer-Tropsch Co-Re-based catalysts. We foresee our developed understanding of the preparation of well-defined nanostructured Co-Re/Al_2O_3/NiAl(110) surfaces to be particularly useful for further fundamental reactivity studies of catalytic reactions by means of surface sensitive probes as high-pressure STM[17], infrared spectroscopy and near-ambient pressure XPS. We are convinced that systematic operando studies in CO-, H_2- and H_2+CO-containing atmospheres on such surfaces will address open questions on the role and location of Re during the reaction, as well as the growth of the long hydrocarbon chains on Co(0001) recently reported by Navarro et al. using the Reactor STM.[5] Finally, it is worth pointing out that both Co and Re nanoparticles have applications beyond FT-catalysis (e.g. NH_3-synthesis[46-47]), and that the reported findings will be of relevance for a wide audience.

Supporting information. Additional STM images and XP spectra, not-normalized XPS quantification, estimation of uncertainties, model details for as-prepared and annealed particles, and references 17, 21 in full are described in the supporting information.

Acknowledgements. Authors (O.I. and A.O.S.) appreciate fruitful scientific discussions with Helmer Fjellvåg. O.I. acknowledges support by the industrial Catalysis Science and Innovation Centre (iCSI), which receives financial support from the Research Council of Norway (contract No. 237922). R.M. acknowledges support by a Dutch SmartMix grant and by NIMIC partner

organizations through NIMIC, a public–private partnership. I.M.N.G. acknowledges the Dutch organization for scientific research (NWO-STW) for her Veni fellowship.

Corresponding author: Anja O. Sjåstad, a.o.sjastad@kjemi.uio.no

References

1. Rytter, E.; Holmen, A., Deactivation and Regeneration of Commercial Type Fischer-Tropsch Co-Catalysts-A Mini-Review. *Catalysts* **2015,** *5*, 478-499.

2. Price, S. W. T.; Martin, D. J.; Parsons, A. D.; Sławiński, W. A.; Vamvakeros, A.; Keylock, S. J.; Beale, A. M.; Mosselmans, J. F. W., Chemical Imaging of Fischer-Tropsch Catalysts under Operating Conditions. *Sci. Adv.* **2017,** *3*, e1602838.

3. Diehl, F.; Khodakov, A. Y., Promotion of Cobalt Fischer-Tropsch Catalysts with Noble Metals: a Review. *Oil Gas Sci. Tech. - Rev. IFP* **2009,** *64*, 11-24.

4. Rytter, E.; Skagseth, T. H.; Eri, S.; Sjåstad, A. O., Cobalt Fischer−Tropsch Catalysts Using Nickel Promoter as a Rhenium Substitute to Suppress Deactivation. *Ind. Eng. Chem. Res.* **2010,** *49*, 4140-4148.

5. Navarro, V.; van Spronsen, M. A.; Frenken, J. W. M., In situ Observation of Self-Assembled Hydrocarbon Fischer–Tropsch Products on a Cobalt Catalyst. *Nat. Chem.* **2016,** *8*, 929-934.

6. Voronov, A.; Tsakoumis, N. E.; Hammer, N.; van Beek, W.; Emerich, H.; Rønning, M., The State and Location of Re in Co–Re/Al_2O_3 Catalysts during Fischer–Tropsch Synthesis:

Exploring High-Energy XAFS for in situ Catalysts Characterisation. *Catal. Today* **2014,** *229*, 23-33.

7. Jacobs, G.; Chaney, J. A.; Patterson, P. M.; Das, T. K.; Davis, B. H., Fischer–Tropsch Synthesis: Study of the Promotion of Re on the Reduction Property of Co/Al_2O_3 Catalysts by in situ EXAFS/XANES of Co K and Re LIII Edges and XPS. *Appl. Catal., A* **2004,** *264*, 203-212.

8. Bakken, V.; Bergene, E.; Rytter, E.; Swang, O., Bimetallic Cobalt/Rhenium Systems: Preferred Position of Rhenium Through an Interdisciplinary Approach. *Catal. Lett.* **2010,** *135*, 21-25.

9. Zacharaki, E. B., M.; Kalyva, M.; Kooyman, P. J.; Fjellvåg, H.; Sjåstad, A.O., Cobalt–Rhenium β-Mn-type Bimetallic Nanoparticles Prepared via Colloidal Chemistry. *in preparation for submission* **2018**.

10. Jaeger, R. M.; Kuhlenbeck, H.; Freund, H. J.; Wuttig, M.; Hoffmann, W.; Franchy, R.; Ibach, H., Formation of a Well-Ordered Aluminium Oxide Overlayer by Oxidation of NiAl(110). *Surf. Sci.* **1991,** *259*, 235-252.

11. Mom, R. V.; Rost, M. J.; Frenken, J. W. M.; Groot, I. M. N., Tuning the Properties of Molybdenum Oxide on Al_2O_3/NiAl(110): Metal versus Oxide Deposition. *J. Phys. Chem., C* **2016,** *120*, 19737-19743.

12. Bäumer, M.; Freund, H.-J., Metal Deposits on Well-Ordered Oxide Films. *Prog. Surf. Sci.* **1999,** *61*, 127-198.

13. Bäumer, M.; Frank, M.; Heemeier, M.; Kühnemuth, R.; Stempel, S.; Freund, H. J., Nucleation and Growth of Transition Metals on a Thin Alumina Film. *Surf. Sci.* **2000,** *454–456*, 957-962.

14. Napetschnig, E.; Schmid, M.; Varga, P., Pd, Co and Co–Pd Clusters on the Ordered Alumina Film on NiAl(110): Contact Angle, Surface Structure and Composition. *Surf. Sci.* **2007,** *601*, 3233-3245.

15. Galhenage, R. P.; Xie, K.; Yan, H.; Seuser, G. S.; Chen, D. A., Understanding the Growth, Chemical Activity, and Cluster–Support Interactions for Pt–Re Bimetallic Clusters on TiO_2(110). *J. Phys. Chem., C* **2016,** *120*, 10866-10878.

16. Heemeier, M.; Stempel, S.; Shaikhutdinov, S. K.; Libuda, J.; Bäumer, M.; Oldman, R. J.; Jackson, S. D.; Freund, H. J., On the Thermal Stability of Metal Particles Supported on a Thin Alumina Film. *Surf. Sci.* **2003,** *523*, 103-110.

17. Herbschleb, C. T.; van der Tuijn, P. C.; Roobol, S. B.; Navarro, V.; Bakker, J. W.; Liu, Q.; Stoltz, D.; Cañas-Ventura, M. E.; Verdoes, G.; van Spronsen, M. A., et al., The ReactorSTM: Atomically Resolved Scanning Tunneling Microscopy under High-Pressure, High-Temperature Catalytic Reaction Conditions. *Rev. Sci. Instrum.* **2014,** *85*, 083703.

18. Surface Preparation Laboratory. Zaandam, the Netherlands.

19. Spronsen, M. A. v. Oxidation Catalysis on Pt and Au. University of Leiden, Delft-Leiden, 2016.

20. LISE laboratory of the Facultes Universitaires Notre-Dame de la Paix, N., Belgium, Least-Squares Curve Fitting Program Winspec.

21. Rost, M. J.; Crama, L.; Schakel, P.; van Tol, E.; van Velzen-Williams, G. B. E. M.; Overgauw, C. F.; ter Horst, H.; Dekker, H.; Okhuijsen, B.; Seynen, M., et al., Scanning Probe Microscopes Go Video Rate and Beyond. *Rev. Sci. Instrum.* **2005,** *76*, 053710.

22. Leiden Probe Microscopy. Leiden, the Netherlands.

23. Nečas, D.; Klapetek, P., Gwyddion: an Open-Source Software for SPM Data Analysis. *Open Phys.* **2012,** *10*, 181-188.

24. Kresse, G.; Schmid, M.; Napetschnig, E.; Shishkin, M.; Köhler, L.; Varga, P., Structure of the Ultrathin Aluminum Oxide Film on NiAl(110). *Science* **2005,** *308*, 1440-1442.

25. Worren, T.; Højrup Hansen, K.; Lægsgaard, E.; Besenbacher, F.; Stensgaard, I., Copper Clusters on Al_2O_3/NiAl(110) Studied with STM. *Surf. Sci.* **2001,** *477*, 8-16.

26. Bäumer, M.; Biener, J.; Madix, R. J., Growth, Electronic Properties and Reactivity of Vanadium Deposited onto a Thin Alumina Film. *Surf. Sci.* **1999,** *432*, 189-198.

27. Venables, J. A.; Harding, J. H., Nucleation and Growth of Supported Metal Clusters at Defect Sites on Oxide and Halide (001) Surfaces. *J. Cryst. Growth* **2000,** *211*, 27-33.

28. Nilius, N.; Ernst, N.; Freund, H. J., Photon Emission Spectroscopy of Individual Oxide-Supported Silver Clusters in a Scanning Tunneling Microscope. *Phys. Rev. Lett.* **2000,** *84*, 3994-3997.

29. Vitos, L.; Ruban, A. V.; Skriver, H. L.; Kollár, J., The Surface Energy of Metals. *Surf. Sci.* **1998,** *411*, 186-202.

30. Robie, R. A.; Hemingway, B. S.; Fisher, J. R., Thermodynamic properties of minerals and related substances at 298.15 K and 1 bar (105 pascals) pressure and at higher temperatures. *U. S. Geological Survey* **1978,** *Bulletin 1452*.

31. Okal, J.; Tylus, W.; Kępiński, L., XPS study of Oxidation of Rhenium Metal on γ-Al_2O_3 Support. *J. Catal.* **2004,** *225*, 498-509.

32. Ramstad, A.; Strisland, F.; Raaen, S.; Worren, T.; Borg, A.; Berg, C., Growth and Alloy Formation Studied by Photoelectron Spectroscopy and STM. *Surf. Sci.* **1999,** *425*, 57-67.

33. Wertheim, G. K., Core-Electron Binding Energies in Free and Supported Metal Clusters. *Eur. Phys. J., B* **1987,** *66*, 53-63.

34. Richter, B.; Kuhlenbeck, H.; Freund, H. J.; Bagus, P. S., Cluster Core-Level Binding-Energy Shifts: The Role of Lattice Strain. *Phys. Rev. Lett.* **2004,** *93*, 026805.

35. Aruna, I.; Mehta, B. R.; Malhotra, L. K.; Shivaprasad, S. M., Size Dependence of Core and Valence Binding Energies in Pd Nanoparticles: Interplay of Quantum Confinement and Coordination Reduction. *J. Appl. Phys.* **2008,** *104*, 064308.

36. Corain, B.; Schmid, G.; Toshima, N., Editorial. In *Metal Nanoclusters in Catalysis and Materials Science*, Elsevier: Amsterdam, 2008; p vii.

37. Lykhach, Y.; Kozlov, S. M.; Skala, T.; Tovt, A.; Stetsovych, V.; Tsud, N.; Dvorak, F.; Johanek, V.; Neitzel, A.; Myslivecek, J., et al., Counting Electrons on Supported Nanoparticles. *Nat. Mater.* **2016,** *15*, 284-288.

38. Wilson, A.; Bernard, R.; Vlad, A.; Borensztein, Y.; Coati, A.; Croset, B.; Garreau, Y.; Prévot, G., Epitaxial Growth of Bimetallic Au-Cu Nanoparticles on TiO_2 (110) Followed in situ

by Scanning Tunneling Microscopy and Grazing-Incidence X-Ray Diffraction. *Phys. Rev. B.* **2014,** *90*, 075416.

39. Felicissimo, M. P.; Martyanov, O. N.; Risse, T.; Freund, H.-J., Characterization of a Pd–Fe Bimetallic Model Catalyst. *Surf. Sci.* **2007,** *601*, 2105-2116.

40. Koester, W. H., E., Zustandsbild und Gitterkonstanten der Legierungen des Kobalts mit Rhenium, Ruthenium, Osmium, Rhodium und Iridium. *Z. Metallk.* **1952,** *43*, 444-449.

41. Gorr, B.; Trindade, V.; Burk, S.; Christ, H.-J.; Klauke, M.; Mukherji, D.; Rösler, J., Oxidation Behaviour of Model Cobalt-Rhenium Alloys During Short-Term Exposure to Laboratory Air at Elevated Temperature. *Oxid. Met.* **2009,** *71*, 157-172.

42. Parschau, M.; Christmann, K., Cobalt on Rhenium(0001) – an Example of Thermally Activated Layer Intermixing and Surface Alloying. *Surf. Sci.* **1999,** *423*, 303-323.

43. Wachi, F. M.; Gilmartin, D. E., Vapor Pressure and Heat of Vaporization of Cobalt. *J. Chem. Phys.* **1972,** *57*, 4713-4716.

44. Ruban, A. V.; Skriver, H. L.; Nørskov, J. K., Surface Segregation Energies in Transition-Metal Alloys. *Phys. Rev. B.* **1999,** *59*, 15990-16000.

45. Bakken, V.; Swang, O., Atomistic and Electronic Structure of Bimetallic Cobalt/Rhenium Clusters from Density Functional Theory Calculations. *J. Chem. Phys.* **2008,** *128*, 084712.

46. Kojima, R.; Aika, K.-i., Cobalt Molybdenum Bimetallic Nitride Catalysts for Ammonia Synthesis: Part 1. Preparation and Characterization. *Appl. Catal., A* **2001,** *215*, 149-160.

47. McAulay, K.; Hargreaves, J. S. J.; McFarlane, A. R.; Price, D. J.; Spencer, N. A.; Bion, N.; Can, F.; Richard, M.; Greer, H. F.; Zhou, W. Z., The Influence of pre-Treatment Gas Mixture upon the Ammonia Synthesis Activity of Co–Re Catalysts. *Catal. Commun.* **2015,** *68*, 53-57.

TOC Graphic

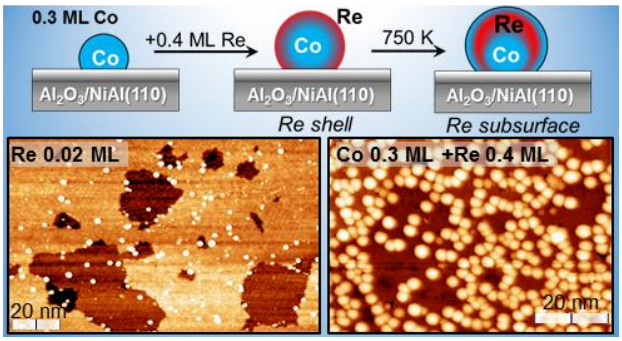
0.3 ML Co
Co
+0.4 ML Re
Re
Co
750 K
Re
Co
Al2O3/NiAl(110)
Al2O3/NiAl(110)
Al2O3/NiAl(110)
Re shell
Re subsurface
Re 0.02 ML
20 nm
Co 0.3 ML +Re 0.4 ML
20 nm